Kinetics and Catalysis, Vol. 46, No. 5, 2005, pp. 743–751. Translated from Kinetika i Kataliz, Vol. 46, No. 5, 2005, pp. 787–794.

Fischer–Tropsch Catalysts Based on Zr–Fe Intermetallides Encapsulated in an Al_2O_3/Al Matrix

A. E. Kuz'min*, Yu. N. Dyatlova, S. F. Tikhov**, V. I. Kurkin*, V. A. Sadykov**, E. V. Slivinskii*†, E. I. Bogolepova*, S. V. Tsybulya**, V. B. Fenelonov**, V. P. Mordovin*, G. S. Litvak**, and A. N. Salanov****

** Topchiev Institute of Petrochemical Synthesis, Russian Academy of Sciences, Moscow, 117912 Russia*

*** Boreskov Institute of Catalysis, Siberian Branch, Russian Academy of Sciences, Novosibirsk, 630090 Russia*

Received October 11, 2004

Abstract—ZrFe and $ZrFe_2$ intermetallides in an Al_2O_3/Al cermet matrix are reported as catalysts for the fixed-bed Fischer–Tropsch synthesis, and the effects of some preparation conditions on their texture, structural, mechanical, and catalytic properties are discussed. A nonmonotonic dependence of their catalytic activity on the size of interametallide particles is observed. The selectivity, activity, and mechanical strength of the composites depend on the calcination temperature and on the place of the hydriding step in the catalyst preparation procedure. In terms of volumetric efficiency, the catalysts prepared are comparable with bulk, unencapsulated intermetallides and are among the most efficient iron-containing catalysts known to date.

INTRODUCTION

The Fischer–Tropsch synthesis (FTS) of hydrocarbons is being increasingly viewed as the most important alternative to their production from petroleum, a fossil fuel that is rapidly being exhausted [1]. This reaction produces a variety of products and makes use of a wide variety of catalysts. Intermetallides and their hydrides are promising catalysts for fixed-bed reactors [2, 3]. Among them, the iron–zirconium system has attracted the greatest attention. It has been reported to show the highest condensable-product (C_{5+}) efficiency per unit volume of the bulk catalyst (200 g l^{-1} h^{-1} at 320°C and 20 MPa [3]). However, the rapid coke formation on these intermetallide catalysts degrades their operating stability and, therefore, restricts their application [4].

In this connection, the improvement of the intermetallide catalysts by their encapsulation in an Al_2O_3/Al cermet matrix is promising. This method not only enhances the operating stability of intermetallide catalysts but also increases their activity several times owing to the fact that the encapsulated intermetallide is divided more finely and, accordingly, possesses a larger accessible surface area, as has recently been shown for the hydrided system $Zr_{0.5–2.6}Fe(H)$ [5–7]. The efficiencies of pure and encapsulated intermetallides change nonmonotonically with composition and peak at an atomic ratio of Zr/Fe = 1 : 1 [7]. As a rule, the selectivity of such catalysts does not change substantially with composition. However, although composite catalysts are superior to the corresponding pure intermetallides in terms of weight efficiency, they have a lower volumetric efficiency and, therefore, need further improvement [6, 7]. This study is aimed at increasing the catalyst efficiency by varying some synthesis conditions, specifically, heat-treatment temperature, the fractional makeup of the active component (AC), and the place of the AC hydriding step in the preparation procedure. Furthermore, we studied the relationship between the physicochemical properties of the catalysts and their performance in FTS.

EXPERIMENTAL

The ACs of the catalysts, which are hydrogenated iron–zirconium intermetallides, were synthesized by alloying the metals in an arc furnace followed by hydriding and passivation (the synthesis is detailed elsewhere [6, 7]).

The ACs were encapsulated in an Al_2O_3/Al matrix by the hydrothermal treatment (HTT) of a mixture of an appropriate AC size fraction and aluminum powder (PA-4 grade for 30 wt % AC and PAHP grade for 50 wt % AC) in a special-purpose die at 100°C followed by the calcination of the granulated product in air at 350 or 550°C. This preparation procedure is described in detail in [5, 8]. Encapsulation was completed after intermetallide hydriding unless otherwise stated.

Catalytic activity in FTS was measured at 300–305°C and a pressure of 3 MPa. The composition of synthesis-gas was $H_2/CO \approx 2 : 1$, the VHSV was 6500–7500 h^{-1}, and the particle size of the catalyst was 2–3 mm. Hydrocarbons in the exhaust gas and in the liquid product were analyzed on a Chrom-5 chromatograph using a flame-ionization detector, temperature

† Deceased.

0023-1584/05/4605-0743 © 2005 MAIK "Nauka/Interperiodica"

Table 1. Effect of the calcination temperature on the properties of the catalyst $ZrFeH_x/Al_2O_3/Al$

Property	Calcination temperature, °C	
	350	550
Total CO conversion, %	46.7	24.4
Conversion of CO to CO_2, %	10.1	2.6
Hydrocarbon yield, g (kg Cat)$^{-1}$ h^{-1}	632	381
g (l Cat)$^{-1}$ h^{-1}	674	338
Hydrocarbon yield on the initial AC basis, g (kg AC)$^{-1}$ h^{-1}	1264	762
CH_4 selectivity, %	29.2	34.9
C_2–C_4 selectivity, %	45.5	39.3
C_{5+} selectivity, %	24.9	25.9
Bulk density, g/cm^3	1.06	0.88
Mechanical strength, MPa	2.1	0.8
Total pore volume, cm^3/g	0.22	0.64
Specific surface area, m^2/g:		
composite catalyst	42	42
unencapsulated $ZrFeH_x$	0.22	–
Micropore and mesopore volume, cm^3/g:		
composite catalyst	0.050	0.051
unencapsulated $ZrFeH_x$	0.012	–
Mean pore diameter up to 2000 Å:		
composite catalyst	39	49
unencapsulated $ZrFeH_x$	440	–

Note: The AC size fraction is 0.25–0.50 mm; $ZrFeH_x/Al_{PAHP} = 1 : 1$.

programming, and a variety of columns. The feed and exit gases were analyzed for unreacted CO and CO_2 on an LKhM-80 chromatograph with a thermal conductivity detector.

The phase composition of catalysts was determined on a URD-63 diffractometer using CuK_α radiation. The total pore volume was estimated from apparent and true density data (determined with a helium Autopycnometer 1320 Micromeritics picnometer). Specific surface area and details of texture were derived from nitrogen adsorption–desorption isotherms [6] on an ASAP-2400 (Micromeritics) instrument. Differential thermal and thermogravimetric analyses were made on a Q-1500D thermoanalytical system (Hungary) in the temperature range 20–700°C at a heating rate of 10 K/min. The crushing strength of samples along the generating line of pellets 9 mm in diameter and 4 mm in height was measured with a Prochnometr PK-1 instrument. Electron micrographs were obtained on an LEO-1430 scanning electron microscope.

RESULTS AND DISCUSSION

The AC most efficient in FTS is $ZrFeH_x$; for this reason, our study was focused on composites based on this AC. The exceptions are the experiments in which the place of the hydriding step in the catalyst preparation sequence was changed, as well as the strength tests for $ZrFe_2$ in the Al_2O_3/Al matrix.

Effect of Calcination Temperature

Table 1 lists the physicochemical properties of $ZrFeH/Al_2O_3/Al$ catalysts resulting from the calcination of the HTT product at various temperatures. For comparison, we present texture parameters for the hydrided intermetallide $ZrFeH_x$ prepared without calcination. These data indicate a significant difference in catalytic properties: as the calcination temperature is increased, the total efficiency of the catalyst decreases by a factor larger than 1.5, while the selectivity remains invariable, although there is some increase in the methane content.

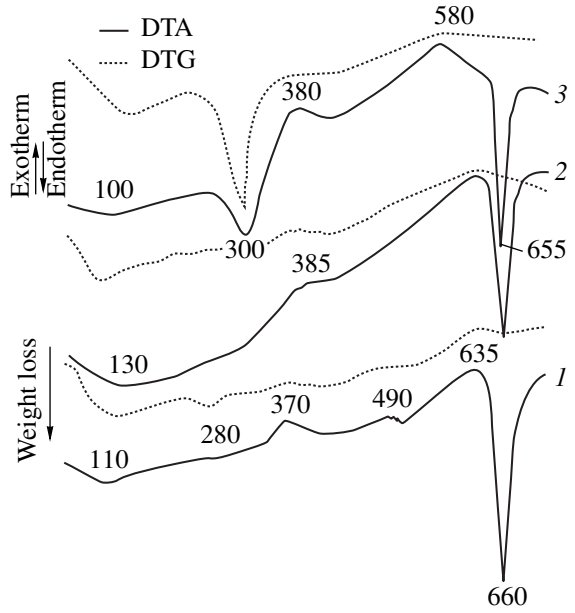

Fig. 1. DTA and DTG curves of the HTT products (0.25- to 0.50-mm AC fraction) for various batch compositions: (*1*) $ZrFe/Al_{PA\text{-}4}$ = 3 : 7, (*2*) $ZrFeH_x/Al_{PA\text{-}4}$ = 3 : 7, and (*3*) $ZrFeH_x/Al_{PAHP}$ = 1 : 1. The peak temperatures are in °C.

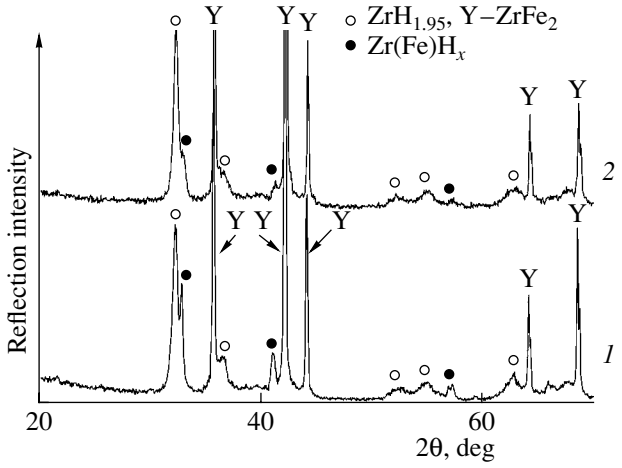

Fig. 2. X-ray diffraction patterns from unencapsulated $ZrFeH_x$ with a particle size of (*1*) 0.25–0.50 and (*2*) <0.04 mm.

The thermoanalytical curves of the HTT products show endotherms, which are accompanied by a weight loss due to the release of adsorbed water (100–130°C) and to the thermal decomposition of the bayerite (~300°C) and pseudoboehmite (~450°C) phases (Fig. 1, curves *3*). All specimens are characterized by an endotherm (655–660°C) due to the melting of aluminum and by an exotherm (580–635°C) due to the oxidation of the aluminum surface. Another exotherm, accompanied by a weight gain, is observed at 360–380°C, which is likely to be due to the bulk oxidation of the AC. No features assignable to hydrogen loss by the hydride phase are seen on the thermoanalytical curves, apparently because the hydrogen content of the samples is low (0.3 wt % in pure AC). These phenomena are typical of other types of composite catalyst based on iron–zirconium alloys (Fig. 1, curves *1*, *2*). Hence, thermal treatment at 350°C results in bayerite decomposition but causes no bulk oxidation of the AC.

Indeed, according to XRD data, the original AC treated with hydrogen contains tetragonal zirconium hydride (ε-$ZrH_{1.95}$) [9], cubic intermetallide $ZrFe_2$ [10], and an unknown zirconium hydride phase with altered unit cell parameters, which is likely to contain iron (Zr(Fe)H) and to be the precursor responsible for the high activity of this AC [7] (Fig. 2). After encapsulation in the Al_2O_3/Al matrix and calcination at 550°C, the resulting composite contains zirconium oxide (monoclinic and tetragonal modifications) and γ-Al_2O_3 along with α-Fe_2O_3 and aluminum. Therefore, thermal treatment during encapsulation results in complete AC oxidation yielding well-crystallized products. After calcination at 350°C, the diffraction pattern of the sample is dominated by reflections from aluminum metal and from traces of iron hydroxide. The other components are likely to be amorphous. This finding is not explained by the effect of the Al_2O_3/Al matrix on the phase transitions in the AC, since the same effect is observed for pure $ZrFeH_x$. Calcination at 350°C produces no noticeable cracks in the particles and no increase in the active surface area, as is suggested by the similar texture parameters (specific surface area and pore volume) of the original and calcined ACs.

Therefore, the dependence of catalytic activity on the calcination temperature can be due to the formation at high temperature of large particles of oxidized iron, which is believed to be less active in FTS (it is well known that iron and cobalt oxides are either inactive in FTS or less active than the respective metals [11]). Moreover, it was shown [2] for the NiZr and CoZr systems that it is the combination of a hydride phase in the bulk and a finely divided transition metal oxide in the surface layer of zirconia that is responsible for the enhanced activity of intermetallide hydrides after reduction–oxidation treatment.

The practical value of granulated catalysts is determined not only by their catalytic properties but also by their mechanical characteristics (strength). The mechanical strength of $ZrFeH/Al_2O_3$/Al decreases with increasing calcination temperature (Table 1). The microstructures and mesostructures of alumina that determine the specific surface area and micropore and mesopore volumes of the composite remain almost unchanged. Only an increase in the total pore volume is observed, which is due to ultramicropores (Table 1). This phenomenon, as well as the dependence of catalytic activity on the calcination temperature, is due to AC oxidation. The deep oxidation of AC particles substantially increases their volume, leading to the crack-

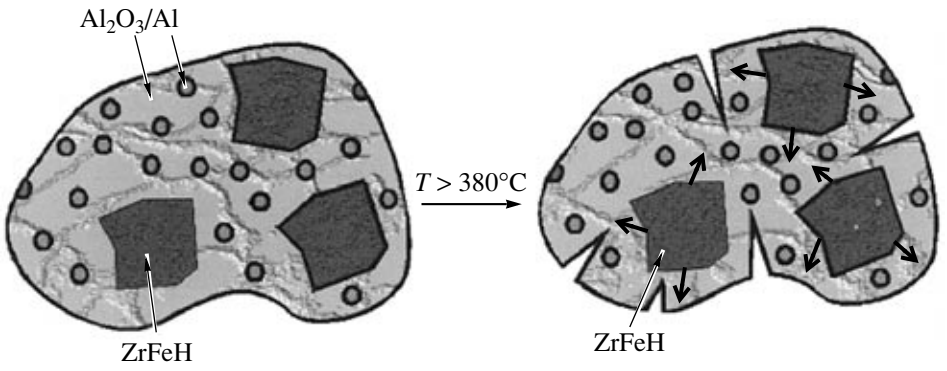

Fig. 3. Processes occurring in the composite catalysts during thermal treatment above 350°C.

ing of the Al_2O_3/Al matrix and to an increase in the ultramicropore size according to the scheme presented in Fig. 4.

The dependence of the mechanical strength on the heat-treatment temperature was studied in more detail for the unhydrided intermetallide $ZrFe_2$ encapsulated in the alumina matrix with the use of PA-4 powder, which is less reactive than PAHP [7]. As is seen in Fig. 4, as the HTT temperature increases from 150 to 550°C, the mechanical strength of the product passes through a maximum at 350°C. According to thermoanalytical data, a weight gain is observed above 350°C, which is due to the bulk oxidation of AC particles, as in the case of the composite with the hydrogenated intermetallide ZrFeH. The difference between the oxidation behaviors of particles is due to both the difference in iron content and the presence (or absence) of a hydrogen treatment step (the latter is discussed below). All these factors also exert an effect on aluminum oxidation during HTT, which, in turn, affects the formation of aluminum hydroxides and AC oxidation during thermal treatment (Figs. 1, 5).

Part of the contacts in the composite yields crystalline phases as early as at the HTT stage owing to transfer processes [12] and self-pressing [13], resulting in a high strength of the composite granules just after drying (Fig. 3). Calcination at 350°C transforms the coagulation contacts remaining after drying to phase contacts, resulting in a further strengthening of the granules. Calcination at 550°C is accompanied by the bulk oxidation of the AC particles, an increase in their sizes, and a decrease in the mechanical strength because of the cracking of the granules. This feature is common to all encapsulated intermetallides and should be taken into account when choosing heat-treatment conditions.

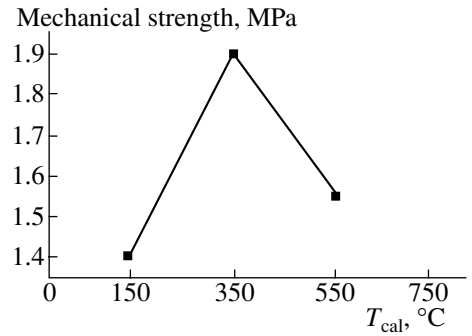

Fig. 4. Mechanical strength of the composite $ZrFe_2/Al_2O_3/Al$ ($ZrFe_2/Al_{PA\text{-}4}$ = 3 : 7; AC particle size, 0.25–0.50 mm) vs. calcination temperature.

Effect of the Particle Size of the Active Component

A decrease in the particle size of the AC from 0.25–0.50 mm to <0.04 mm at the same composition of the initial mixture (1 : 1) and calcination temperature (350°C) does not result in any substantial increase in FTS activity (Tables 1, 2). On the contrary, the total efficiency with respect to hydrocarbons first decreases, and only the efficiency of the catalyst with the finest AC exceeds the efficiency of the composite with the most coarse AC fraction. The total efficiency with respect to

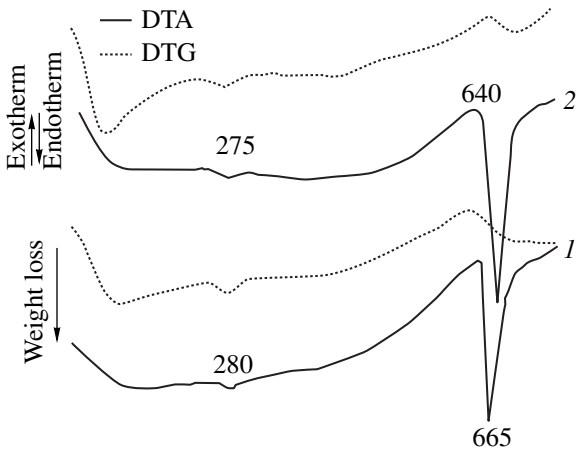

Fig. 5. DTA and DTG curves of the HTT products of aluminum (PA-4)–intermetallide mixtures (7 : 3): (*1*) $ZrFe_2$ and (*2*) $ZrFe_2H$. The AC size fraction is 0.25–0.50 mm. Temperature is in °C.

Table 2. Effect of the particle size of the AC on the properties of the catalyst $ZrFeH_x/Al_2O_3/Al$

Property	AC particle size, mm		
	0.20–0.25	0.056–0.08	<0.04
Total CO conversion, %	44.1	38.4	54.9
Conversion of CO to CO_2, %	10.9	5.8	15.4
Hydrocarbon yield, g (kg Cat)$^{-1}$ h^{-1}	570	467	678
g (l Cat)$^{-1}$ h^{-1}	584	443	694
Hydrocarbon yield on the basis of the initial AC, g (kg AC)$^{-1}$ h^{-1}	1140	934	1356
CH_4 selectivity, %	32.9	30.9	35.5
C_2–C_4 selectivity, %	44.6	43.5	44.4
C_{5+} selectivity, %	22.5	25.6	20.1
Bulk density, g/cm^3	1.02	0.94	1.02
Mechanical strength, MPa	1.4	0.9	2.1
Total pore volume, cm^3/g	0.28	0.31	0.23
Specific surface area, m^2/g:			
composite catalyst	49	25	36
unencapsulated $ZrFeH_x$	0.12	0.21	0.04
Micropore and mesopore volume, cm^3/g:			
composite catalyst	0.036	0.023	0.032
unencapsulated $ZrFeH_x$	0.0004	0.0007	0.0002
Mean pore diameter up to 2000 Å:			
composite catalyst	30	37	35
unencapsulated $ZrFeH_x$	140	134	120

Note: $ZrFeH_x/Al_{PAHP}$ = 1 : 1; calcination temperature, 350°C.

C_{5+} hydrocarbons is lower for the catalyst with the finest AC than for the catalyst with the most coarse AC fraction (139.5 versus 167.8 g l^{-1} h^{-1}). In this series of experiments, the selectivities to various hydrocarbon fractions changed slightly and irregularly. It is conventionally expected that specific efficiency will grow, with some degree of regularity, down to an AC particle size of ~0.1 mm or below, starting at which the diffusion of reactants (first of all, CO) in the catalyst micropores and mesopores filled with condensed hydrocarbons has no considerable reducing effect on catalytic activity [14].

Analysis of the texture and mechanical characteristics demonstrates that, as the AC particle size increases, the total pore volume varies only slightly, while the micropore and mesopore volumes, the specific surface area of the catalysts, and the mechanical strength of granules vary nonmonotonically (Tables 1, 2). The mean pore diameter of the AC itself decreases from 440 to 120 Å upon grinding, accompanied by a decrease in specific surface area, whereas the pore volume changes nonmonotonically. The specific surface area of the finest fraction decreases markedly (Table 2). Apparently, grinding can lead either to the cracking of the AC particles or, conversely, to their strengthening due to percussion riveting. The interplay of these processes cannot be controlled at present. Presumably, a decrease in the size of AC particles in the macropore structure of composite catalysts leads to a decrease in the proportion of pores with a size of several tens of micrometers. This is seen on a qualitative level from scanning electron microscopy data for the composites with the most coarse (Fig. 6) and the finest (Fig. 7) AC fractions. Macropores that are formed near AC particles of the 0.20- to 0.25-mm fraction are much larger than macropores that are formed near particles of the <0.04 mm fraction. In any case, as the fractional makeup of the AC is varied, the texture of the composite has a rather slight effect on catalytic efficiency, because the contribution from the macropores to the total pore volume of the catalyst granules is very large.

X-ray crystallography revealed no significant effect of grinding on the phase composition of the AC (Fig. 2). The decrease in the total intensity of the peaks due to

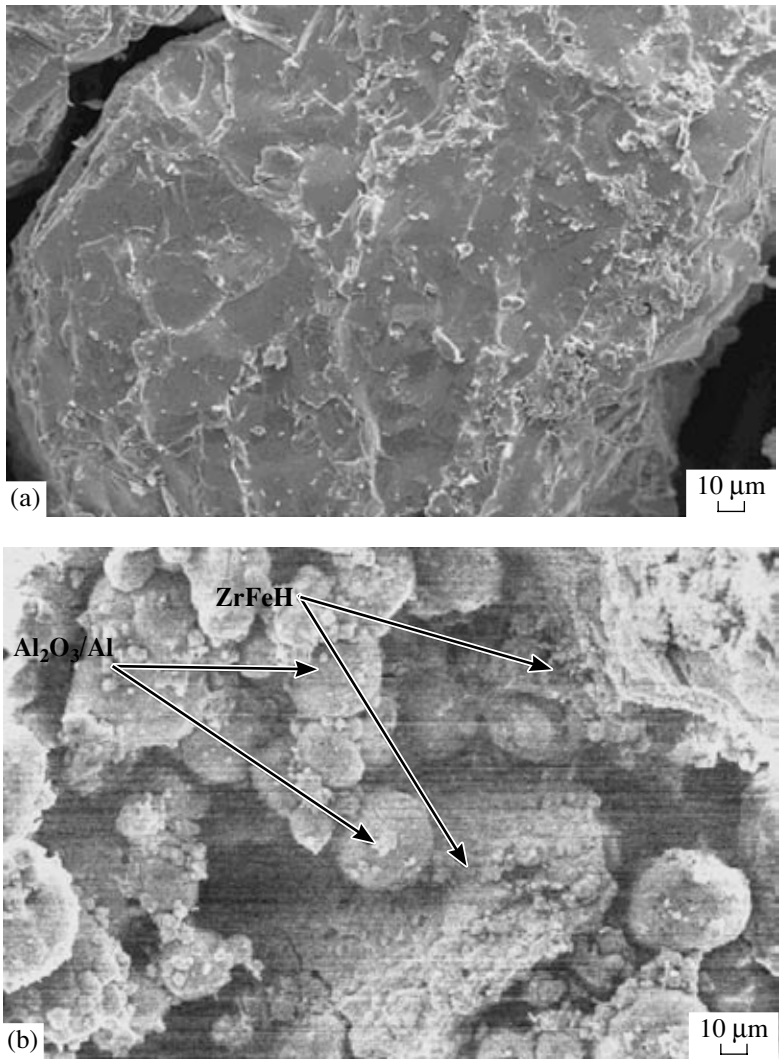

Fig. 6. Electron micrographs of (a) original $ZrFeH_x$ particles (0.20–0.25 mm) and (b) the resulting composite catalyst $ZrFeH_x/Al_2O_3/Al$ (the batch composition is $ZrFeH_x/Al = 1 : 1$).

the fine fraction, which is apparently due to the change in the scattering ability of the sample, is not accompanied by a change in the intensity of the peaks of ZrFeH relative to the intensity of the peaks of other components ($ZrH_{1.95}$).

As follows from thermoanalytical data, the strongest effect of the fractional makeup of the AC is observed for the composite resulting from HTT. The DTA and DTG curves for three samples with a coarse AC fraction, though somewhat different in shape, have a significant common feature, specifically, a sharp peak at 290–300°C, which is due to the decomposition of crystalline bayerite. This peak is missing in the encapsulated catalyst based on the <0.4 mm AC fraction. Presumably, the disperse AC influences aluminum oxidation and the formation of aluminum hydroxides. The reactivity of aluminum and, accordingly, the alumina content of the composite decrease with decreasing particle size. The reduced hydroxide content of the HTT product leads to a greater amount of incompletely oxidized aluminum, which manifests itself as a growth of the endothermic peak at 655°C (Fig. 8, curves *4*). Note that, because PA-4 powder is less reactive than PAHP powder, the PA-4-based composite is characterized by less pronounced thermoanalytical peaks due to aluminum hydroxide decomposition than the PAHP-based composite (Fig. 1) and has a much higher specific activity in terms of pure intermetallides [7].

Therefore, the components influence one another during HTT. The products of the HTT of aluminum can "decorate" the AC surface through chemical interaction between aluminate ions and iron hydroxides that have formed in the alkaline medium [12] and the formation of iron–aluminum mixed oxides. An aluminum hydroxide "coat" may be formed, which can give porous alumina on the AC surface during thermal treatment. This

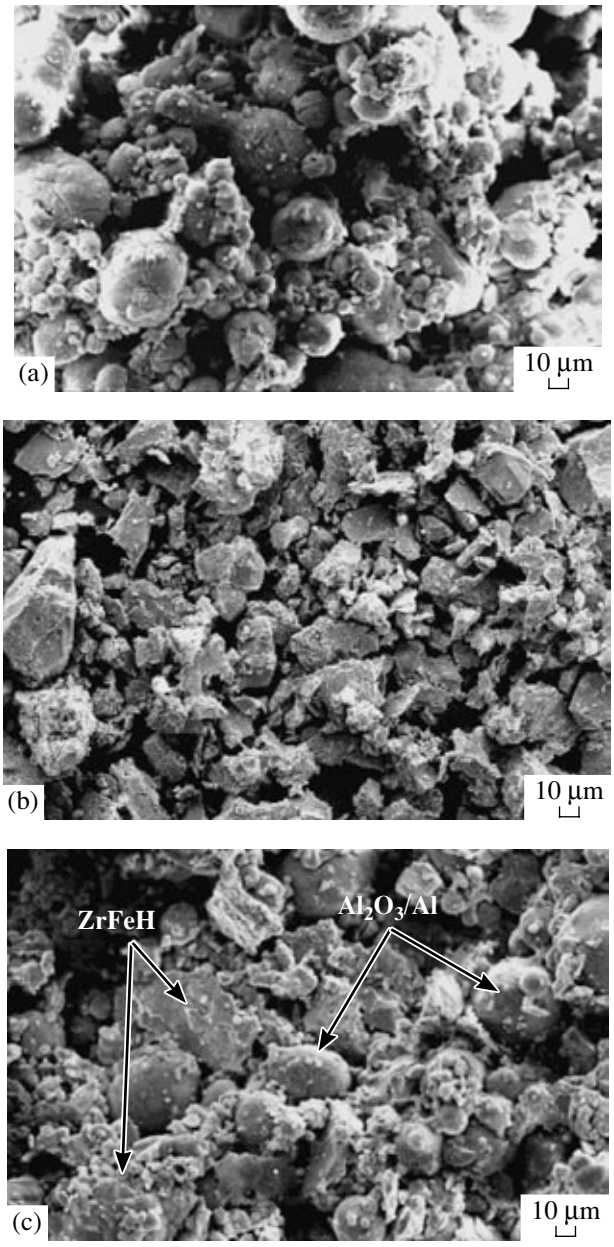

Fig. 7. Electron micrographs of (a) the Al_2O_3/Al matrix, (b) original $ZrFeH_x$ particles (<0.04 mm), and (c) the composite catalyst $ZrFeH_x/Al_2O_3$/Al (the batch composition is $ZrFeH_x/Al_{PAHP} = 1 : 1$).

coating can obstruct both the access of reactants and the removal of products. Both effects would decrease the specific activity (per unit surface area) of the AC and the composite catalysts as a whole if the particle size were to decrease from 0.25–0.50 to 0.06–0.08 mm. On the other hand, the finer AC affects the reactivity of aluminum during HTT and thus decreases the total amount of hydroxo compounds in the pores of the resulting composite. This effect reduces the "decoration" effects and increases the catalytic activity of the <0.04 mm fraction (Tables 1, 2).

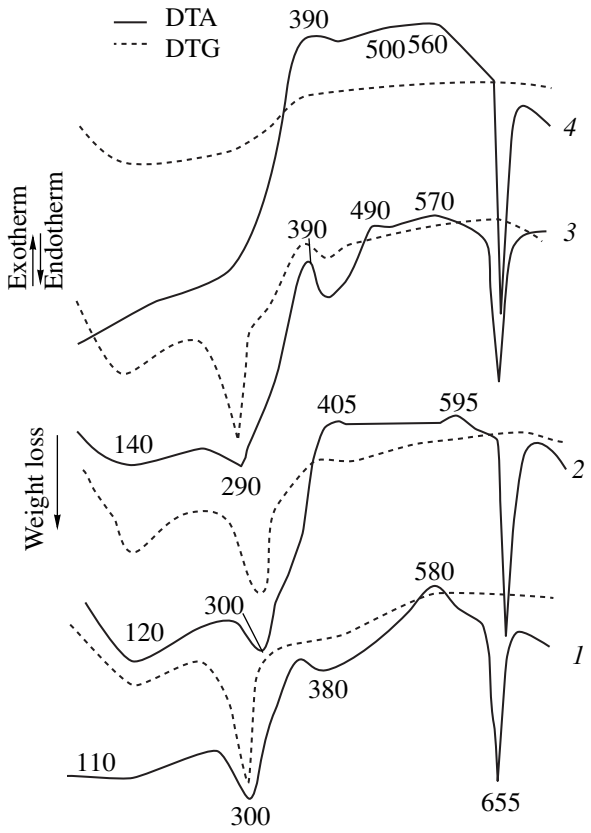

Fig. 8. DTA and DTG curves of the HTT products for various size fractions of the AC in the mixture ($ZrFeH_x/Al_{PAHP} = 1 : 1$): (*1*) 0.25–0.50, (*2*) 0.20–0.25, (*3*) 0.06–0.08, and (*4*) <0.04 mm. Temperature is in °C.

Effect of the Order of the Hydriding and Encapsulation Steps

Generally, the intermetallide can be hydrided either before encapsulation (with passivation) or after encapsulation just before the reaction. Either method has both advantages and drawbacks with respect to catalyst efficiency. For this reason, we studied the effect of the order of the hydriding and encapsulation stages on the properties of the composites obtained from PA-4 powder containing 30% $ZrFe_2$ or ZrFe by calcination at 550°C.

The most unexpected result was obtained for the $ZrFe_2$ AC. When hydriding was performed after encapsulation, the activity of the encapsulated catalyst was unaffected while its selectivity changed dramatically: the proportion of condensed hydrocarbons decreased and the methane selectivity increased by a factor of about 1.5. The original intermetallide consisted of β-Zr, the tetragonal phase Zr_2Fe, and the hexagonal modification of $ZrFe_2$. This intermetallide is almost unhydridable. However, hydrogen treatment caused chemical changes: there occurred phase transformations (zirco-

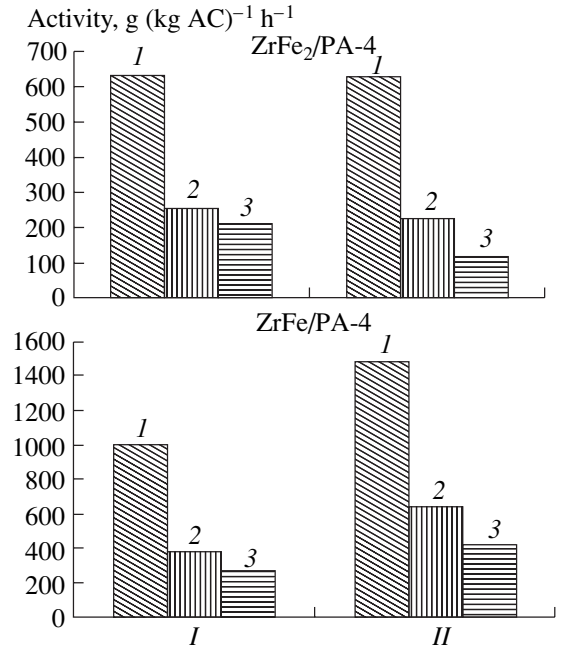

Fig. 9. Effect of the place of the hydriding step in the preparation procedure on the FTS activity of composite catalysts with various ACs (size fraction, 0.25–0.50 mm; batch composition, AC/Al_{PA-4} = 3 : 7; calcination temperature, 550°C): (*I*) hydriding before encapsulation and (*II*) hydriding after encapsulation; (*1*) total activity, (*2*) C_2–C_4 conversion activity, and (*3*) C_{5+} conversion activity.

nium metal and Zr_2Fe disappeared). Note that the composites containing untreated $ZrFe_2$ are markedly stronger than the composites containing hydrogen-pretreated $ZrFe_2$ (compare the data presented in Fig. 3 and [7]).

In the case of ZrFe, interchanging the hydriding and encapsulation stages causes changes in the catalytic properties that are opposite to those observed for $ZrFe_2$. The preliminary hydriding of ZrFe exerts only a slight effect on selectivity. The total activity of the preliminarily hydrided AC is lower than that of the unhidrided AC by a factor of about 1.5 (Fig. 9). This intermetallide contains two phases before treatment, namely, tetragonal Zr_2Fe and cubic $ZrFe_2$. The phases resulting from hydriding are described above.

Therefore, as compared to ZrFe, the tetragonal phase $ZrFe_2$ is more stable and less reactive toward hydrogen. Its bulk oxidation during encapsulation in the Al_2O_3/Al matrix is likely to produce more coarse particles of iron oxide, and the most profound changes in this material occur during calcination. This fact favors methanation. The Zr and Zr_2Fe phases in the Zr/Fe = 1 : 1 AC are hydrided much more readily to yield ε-$ZrH_{1.95}$ and ZrFeH. Apparently, this treatment activates the AC for subsequent oxidation during incapsulation and reduces its FTS activity. Thermal treatment at 550°C results in the irreversible oxidation of the zirconium hydride phase, which plays an important role in the activation of hydrogen [2]. This effect diminishes the catalytic activity observed after hydrogen pretreatment, because the unhidrided intermetallide is oxidized to a lesser extent during incapsulation. As a consequence, iron particles on the surface of this AC are smaller than iron particles in the case of oxidation followed by reduction. After reduction with hydrogen, the smaller oxide particles form more active iron carbides on the surface of zirconium hydride, and these carbides act as complex active sites in the reaction medium [15]. Thus, the complicated processes involved in the formation of the precursor phase depend on the order of redox treatment stages and the optimum order depends on the chemical nature of the AC.

CONCLUSION

Our studies have led us to conclude that the granulation of the ACs based on the iron–zirconium intermetallides does not consist of mechanical encapsulation in the Al_2O_3/Al matrix but is a complicated physicochemical process in which the AC and the matrix are mutually affected. The optimal calcination temperature that favors bayerite decomposition not accompanied by bulk AC oxidation has been determined. Varying the particle size of the AC results in nonmonotonic changes in the catalytic and mechanical properties of the composite. The effect of the place of the hydriding step in the catalyst preparation procedure has been considered, and it has been demonstrated that the hydriding behavior of the intermetallide depends on its composition. The preparation procedure for the encapsulated iron–zirconium intermetallides can be optimized to obtain iron particles of optimal size on the surface. The zirconium-based hydride phase seems to have an effect on the total catalyst activity. The highest volumetric efficiency of the composite catalysts with respect to liquid hydrocarbons (~168 g l^{-1} h^{-1}) is almost equal to the volumetric efficiency of pure hydrides, although the bulk density of the former exceeds the bulk density of the latter by a factor larger than 3. Therefore, these catalysts are among the most efficient iron-containing Fischer–Tropsch catalysts.

ACKNOWLEDGMENTS

This work was supported by the Russian Foundation for Basic Research (project No. 02-03-32277).

REFERENCES

1. Kessel, I.B. and Protasov, N.N., *Katal. Prom–sti*, 2004, no. 5, p. 60.
2. Lunin, V.V. and Khan, A.Z., *J. Mol. Catal.*, 1984, vol. 25, p. 317.
3. Rozovskii, A.Ya., *Kinet. Katal.*, 1999, vol. 40, no. 3, p. 358.
4. Vytnova, L.A., Mordovin, V.P., Kliger, G.A., *et al.*, *Neftekhimiya*, 2002, vol. 42, no. 2, p. 111.

5. Tikhov, S.F., Sadykov, V.A., Potapova, Yu.V., *et al.*, *Stud. Surf. Sci. Catal.*, 1998, vol. 118, p. 797.
6. Tikhov, S.F., Kurkin, V.I., Sadykov, V.A., *et al.*, *Neftekhimiya*, 2003, vol. 43, no. 6, p. 417.
7. Tikhov, S.F., Kurkin, V.I., Sadykov, V.A., *et al.*, *Stud. Surf. Sci. Catal.*, 2004, vol. 147, p. 337.
8. Tikhov, S.F., Potapova, Yu.V., Sadykov, V.A., *et al.*, *React. Kinet. Catal. Lett.*, 2002, vol. 77, no. 2, p. 267.
9. JCPDS File, 36-1339.
10. *JCPDS File*, 18-0666.
11. Slivinskii, E.V., Kuz'min, A.E., Abramova, A.V., *et al.*, *Neftekhimiya*, 1998, vol. 38, no. 4, p. 243.
12. Rat'ko, A.I., Romanenkov, V.E., Bolotnikova, E.V., and Krupen'kina, Zh.V., *Kinet. Katal.*, 2004, vol. 45, no. 1, p. 162.
13. Tikhov, S.F., Fenelonov, V.B., Sadykov, V.A., *et al.*, *Kinet. Katal.*, 2000, vol. 41, no. 6, p. 916.
14. Zimmerman, W.H., Rossin, J.A., and Bukur, D.B., *Ind. Eng. Chem. Res.*, 1989, vol. 28, p. 406.
15. Li, S., Meitzner, G.D., and Iglesia, E., *Stud. Surf. Sci. Catal*, 2001, vol. 136, p. 387.